



## Model-based simulation and validation of small fixed wing UAV

Original  
Article

Ahmed Elbeshbeshy, Ehab Safwat, Mohamed Reda, Ahmed Mohsen Kamel

Military Technical College, Cairo, Egypt

### Keywords:

Dynamic model, GNC, MATLAB (Simulink), small fixed-wing UA, system identification

### Corresponding Author:

Ahmed Elbeshbeshy, Military Technical College, Cairo, Egypt, **Tel.:** 01066702278, **Email:** ahmedelbeshbeshy1@icloud.com

### Abstract

Flight Guidance, Navigation, and Control systems are the crucial core of any flying vehicle, particularly in UAVs. GNC algorithms should be tested and verified using a validated nonlinear 6-DOF model to be evaluated before actual flight. As a result, increasing UAV modeling accuracy and an open-loop simulation model that describes the UAV behaviors for various inputs are highly needed. In this work, a nonlinear model of UAV is proposed. The inertia mass model is validated utilizing experimental measurements using the pendulum method; subsequently, the behavior of the actuators in conjunction with the UAV's deflection component is validated using system identification. Additionally, a test setup has been devised to measure the propulsion model characteristics, and the experimental results are analyzed. The aerodynamic coefficients and derivatives at various angles of attack are estimated using semi-empirical software (DATCOM). The dynamic model is based on motion equations to simulate the overall model. This work advances by incorporating the sub-models mentioned above into a unified open-loop flight simulation model for the UAV based on the improvements made to the previous sub-models. By adopting this integrated approach, we can thoroughly simulate the UAV's behavior under different flight conditions, which assesses the efficiency of our design processes, and the results confirm the accuracy and dependability of each sub-model. Additionally, we analyze the UAV's stability in an open-loop system, considering both lateral and longitudinal aspects, which evaluates the UAV's capacity to maintain balance and respond to control commands in various flying situations, which is crucial in the stability and safety of the UAV in real-world operational settings, hence confirming the overall success of our integrated simulation design.

## 1. INTRODUCTION

Unmanned Aerial Vehicles (UAVs) have become indispensable technological tools, revolutionizing various fields such as military operations, commercial aerial photography, agricultural monitoring, and disaster relief. Their ability to operate in hazardous or inaccessible environments has spurred a surge in research and innovation. Furthermore, UAVs are serving as a catalyst for advancements in autonomous systems and robotics, igniting the imagination of the scientific community. By merging advanced engineering and technology, they are redefining the limits of remote sensing, data collection, and autonomous operations<sup>[1,2]</sup>. The development of an effective autopilot system for fixed-wing UAVs underscores the complexity of modern aerospace engineering. This system, comprising the three main components – Guidance, Navigation, and Control (GNC) – is instrumental in the

UAV's operation<sup>[3]</sup>. The guidance system charts a course for the UAV to ensure it follows a predefined trajectory, the navigation system provides crucial data on its location and orientation, and the control system dynamically adjusts flight parameters to adapt to environmental factors and internal navigational inputs. David van Wyk 2020 depicted these interdependent systems as vital for autonomous UAV flight in the block diagram<sup>[4]</sup>. The absence of GNC would render UAVs incapable of effective navigation or safe mission completion, underscoring its role in ensuring stability and control<sup>[5]</sup>.

The foundation of a reliable GNC system depends on developing high-fidelity simulation models, which is crucial for UAV design and testing. These models enable researchers and engineers to refine control strategies and predict and improve UAV behavior under diverse operational scenarios, ultimately enhancing UAV effectiveness, safety, and operational reliability<sup>[6,7]</sup>. The simulation models for

UAVs are based on kinematic and dynamic equations of motion, rooted in Newtonian physics. These equations provide a mathematical framework that accurately depicts UAV behavior under various forces and movements. The comprehensive UAV dynamics model is divided into five specialized sub-models: geometric and mass inertia, actuation, propulsion, aerodynamic, and atmospheric. Each sub-model targets specific characteristics of UAV operation to ensure a detailed representation of its performance capabilities<sup>[8]</sup>. Each sub-model in our study culminates in extensive aerospace research and technological advancements. Recent developments in the Aerodynamic model provide valuable insights into methods for calculating aerodynamic coefficients for fixed-wing UAVs, emphasizing their importance in design and performance evaluation. Determining aerodynamic coefficients involves a comprehensive design cycle, including aspect ratio, constraint analysis, weight estimation, airfoil selection, and aerodynamics coefficient analysis<sup>[9]</sup>. In 2015, Hassan Alian, Khaki, and Khosravi used computational fluid dynamics (CFD) analyses to specify the aerodynamic coefficients for a civil tilt-rotor VTOL UAV<sup>[10]</sup>. We chose the DATCOM method for its balance of accuracy and simplicity, which instills confidence in our research methodology's robustness.

The geometric and mass inertia model defines the UAV's motion dynamics based on its geometric properties and mass distribution<sup>[11]</sup>. Xu and Shi (2015) emphasized the importance of these characteristics in developing effective control strategies for hypersonic vehicles, while Ryll, Bicego, and Franchi (2016) highlighted their influence on UAV maneuverability and control<sup>[12,13]</sup>. Our research adopts a hands-on approach, using the practical pendulum method to accurately measure mass and inertia, ensuring the reliability of our model in real-world applications. The atmospheric model is a significant aspect of the design and performance of UAVs, which defines a set of standard atmospheric conditions that are assumed to exist at a certain altitude; it includes parameters such as temperature, pressure, and density, which is commonly used as a reference for aircraft design and performance calculations. One common atmospheric model used for UAVs is the International Standard Atmosphere (ISA) model<sup>[14]</sup>.

Chowdhary *et al.* (2013) emphasized the significance of precise actuation system modeling for maintaining safe and stable flight, especially under adverse conditions<sup>[15]</sup>. Our approach extends the validation of the actuation model beyond theory by emphasizing real-time empirical validation through rigorous experimentation to ensure higher reliability and accuracy in our actuation model, crucial for handling real-world uncertainties and challenges in UAV flight dynamics<sup>[16]</sup>. Khawaja *et al.* (2018)

stressed the need for accurate propulsion system modeling to support robust UAV communication during flight<sup>[17]</sup>. Li *et al.* (2014) highlighted the connection between precise navigation systems and propulsion performance, while Freeman *et al.* (2013) underscored the critical importance of fault detection for propulsion system reliability, a factor that significantly reassures us about the safety and reliability of UAVs<sup>[18,19]</sup>. Our approach to developing the propulsion model involved rigorous application of system identification techniques using real-world experimental data to enhance fidelity to actual operational conditions.

This paper presents a comprehensive methodology for developing, simulating, and validating a reliable fixed-wing UAV model. We began by gathering geometry data and using accurate sensors for experimental data collection. The actuation model was validated through real-time tests, a crucial step that provides valuable insights into its operational behavior and reassures the audience about the model's reliability. We used the DATCOM method and Aircraft Intuitive Design (AID) software for aerodynamic modeling, with open-loop flight simulations confirming the model's accuracy. The UAV's mass inertia properties were determined using CAD modeling and the pendulum method, with the latter proving more precise. The propulsion system was modeled using system identification techniques and validated through experimental testing and multi-input data. This meticulous process significantly advances UAV design, laying a foundation for future developments in efficiency and reliability.

The structure of this paper is: Section 2 describes the mathematical model of the airplane. Section 3 discusses the modeling of small UAVs, which includes the geometric and mass inertia model, aerodynamic model, atmospheric model, actuator model, and propulsion model. Section 4 presents all the results of open-loop simulations. Finally, Section 5 represents the conclusion and future work.

## 2- UAV MATHEMATICAL MODEL

The mathematical representation of the airplane is established through the simulation of UAV flight dynamics using nonlinear differential equations. This includes formulating the UAV Equations of Motion and incorporating the aerodynamic forces and moments. Consequently, the model introduces twelve state variables. For instance, three position and velocity state descriptions represent the UAV's translational motion. Similarly, the rotational motion is characterized by three angular positions and three angular velocity states<sup>[20]</sup>. UAV moments and forces are displayed in Figure 1 additionally, the orientation of UAV's, comprising roll, pitch and azimuth, is considered in the model.

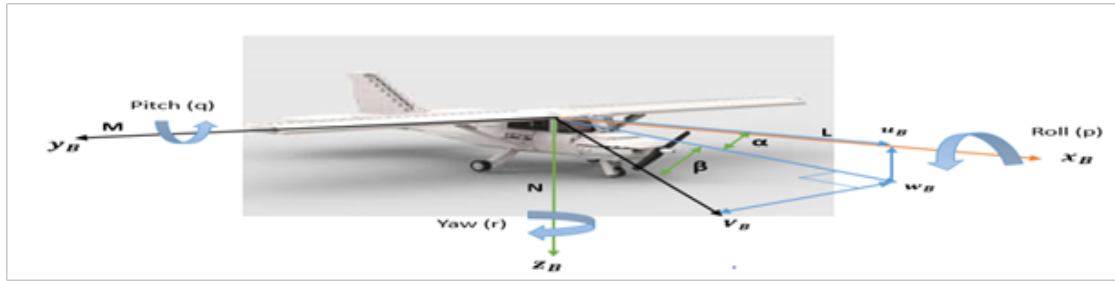


Fig. 1: Moments, forces, and orientations acting on UAV

## 2.1 Kinematic model

This model focuses on the relation between position and velocity, represented by two formulas correlating the linear and angular positions in the inertial frame with the body frame, alongside frame transformation matrices, considering the neglect of forces and moments.

### 2.1.1 Linear motion

The UAV's translational velocity is typically represented using velocity components ( $v_x, v_y, v_z$ ) along each axis within a coordinate frame of the body. However, translational position ( $x, y, z$ ) for UAV is commonly determined and demonstrated in an inertial reference frame. To relate

these velocity vectors in the body frame and the rates of change of position vectors in an inertial frame, a rotational transformation and differentiation are necessary.

$$\frac{d}{dt} \begin{pmatrix} x \\ y \\ z \end{pmatrix} = R_b^i \begin{pmatrix} v_x \\ v_y \\ v_z \end{pmatrix} \quad (1)$$

$x, y$  and  $z$  are the position along the  $x, y$  and  $z$ -axis of the inertial frame respectively.

$v_x, v_y$  and  $v_z$  are the linear velocities of the object along the  $x, y$  and  $z$ -axis of the body respectively.

$R_b^i$ . Matrix for transitioning from the body frame to the inertial frame,

$$\text{Where } R_b^i = \begin{pmatrix} \cos\theta \cos\psi & \sin\phi \sin\theta \cos\psi - \cos\phi \sin\psi & \cos\phi \sin\theta \cos\psi + \sin\phi \sin\psi \\ \cos\theta \sin\psi & \sin\phi \sin\theta \sin\psi + \cos\phi \cos\psi & \cos\phi \sin\theta \sin\psi - \sin\phi \cos\psi \\ -\sin\theta & \sin\phi \cos\theta & \cos\phi \cos\theta \end{pmatrix}$$

### 2.1.2 Angular motion

Describes the relationship between angular positions (Euler angles) ( $\phi, \theta, \psi$ ) characterized from three distinct coordinate frames and angular rates ( $p, q, r$ ) in the body frame.

$$\begin{pmatrix} \dot{\phi} \\ \dot{\theta} \\ \dot{\psi} \end{pmatrix} = R_b^r \begin{pmatrix} p \\ q \\ r \end{pmatrix} \quad (2)$$

$p$  Represent the roll rate, signifies the angular velocity around the  $x$ -axis, known as is the roll axis.

$q$  Represent the pitch rate, indicates the angular velocity around the  $y$ -axis, which corresponds to the pitch axis.

$r$  Represent the yaw rate, denotes the angular velocity about the  $z$ -axis, representing the yaw axis.

$\phi$  Represent the roll angle, the rotation about the  $x$ -axis, which is the roll axis.

$\theta$  Represent the pitch angle, the rotation about the  $y$ -axis.

$\psi$  Represent the yaw angle, the rotation about the  $z$ -axis.

$R_b^r$  Represent the Matrix for converting from frames rotated with respect to the body frame to the body frame.

$$\text{Where } R_b^r = \begin{pmatrix} 1 & \sin\phi \tan\theta & \cos\phi \tan\theta \\ 0 & \cos\phi & -\sin\phi \\ 0 & \frac{\sin\phi}{\cos\theta} & \frac{\cos\phi}{\cos\theta} \end{pmatrix}$$

## 2.2 Dynamic model

This model focuses on the relation between force and moment according to Newton's second law, initially applied to linear degrees of freedom and subsequently extended to angular degrees of freedom, which are held in inertial reference frames. In our work, the earth frame is assumed to be an acceptable flat earth model for small UAVs. As a result, the movement will be converted from the body frame to the Earth frame utilizing rotational matrices. Applying this relation to determine the equations of motion for the UAV<sup>[20]</sup> as:

$$\frac{d}{dt_i} \mathbf{P} = \frac{d}{dt_b} \mathbf{P} + \omega_{b/i} \times \mathbf{P} \quad (3)$$

Which expresses  $p$  derivative in frame  $f_i$  in terms of its change in frame  $f_b$  and two frames relative rotation and  $\omega_{(b/i)}$  express the angular velocity in the inertial frame.

### 2.2.1 Translational motion

When applying the second law of Newton to the body, the equation is expressed as follows:

$$\sum F = \frac{d}{dt_i} (\text{linear momentum}) = m\dot{V}_i \quad (4)$$

$F$  Represents the total of all external forces, such as gravity, aerodynamic forces, and propulsion, controlling on the UAV,  
 $m$  Denotes the mass of the UAV,  $V_i$  represents the inertial frame's velocity's derivative which according to equation (3), can be expressed as a function of the angular velocity and the derivative in the body frame as follows:

$$\frac{dV_b}{dt_i} = \frac{dV_b}{dt_b} + \omega_{b/i} \times V_b \quad (5)$$

$$\sum F_b = m\dot{V}_b + w_{b/i} \times V_b \quad (6)$$

Where  $F_b (f_x, f_y, f_z), V_b (v_x, v_y, v_z)$  and  $w_{b/i} (p, q, r), V_b$  the velocity vector in body frame.

Consequently, the three equations that govern translational dynamics can be outlined as follows:

$$\begin{pmatrix} \dot{v}_x \\ \dot{v}_y \\ \dot{v}_z \end{pmatrix} = \begin{pmatrix} rv_y - qv_z \\ pv_z - rv_x \\ qv_x - pv_y \end{pmatrix} + \frac{1}{m} \begin{pmatrix} f_x \\ f_y \\ f_z \end{pmatrix} \quad (7)$$

### 2.2.2 Rotational motion

The second law of Newton stipulates that:

$$\sum M = \frac{d}{dt_i} (\text{angular momentum}) = \frac{dH}{dt_i} \quad (8)$$

$M$  Illustrates the aggregate of all externally applied moments.

Equation (3) can be used to expand the rate of change of angular momentum w.r.t time in the inertial frame.

$$\sum M_b = \frac{dH_b}{dt} + w_{b/i} \times H_b \quad (9)$$

$H_b$  Refers to angular momentum, which characterized as the result of multiplying the inertia matrix ( $J$ ) by the angular velocity vector.

$$H_b = Jw_{b/i} \quad (10)$$

From equation (9) and (10) we get:

$$\sum M_b = \frac{dJw_{b/i}}{dt} + w_{b/i} \times Jw_{b/i} \quad (11)$$

$$\dot{w}_{b/i} = \begin{pmatrix} \dot{p} \\ \dot{q} \\ \dot{r} \end{pmatrix} = J^{-1} [-w_{b/i} \times (Jw_{b/i}) + M] \quad (12)$$

$$\text{Where, } J = \begin{pmatrix} j_{xx} & j_{xy} & j_{xz} \\ j_{yx} & j_{yy} & j_{yz} \\ j_{zx} & j_{zy} & j_{zz} \end{pmatrix}$$

The diagonal terms of  $J$  represent the moments of inertia, indicating the aircraft's resistance to acceleration around specific axes of rotation. On the other hand, the off-diagonal elements are known as products of inertia. If the airframe exhibits symmetry about two plans, the products of inertia can be safely neglected and assumed to be zero due to their minimal impact,

$$\text{where, } J = \begin{pmatrix} j_{xx} & 0 & 0 \\ 0 & j_{yy} & 0 \\ 0 & 0 & j_{zz} \end{pmatrix}$$

## 3- COMPREHENSIVE MODELING OF A SMALL UAV

The previous section derives the equations required to describe the dynamics of UAVs and obtain an adequate model; this section completes the 6DOF nonlinear model by integrating the UAV sub-models. This enables computer programs to solve mathematical models of UAV flight dynamics produced by forces and moments.

### 3.1 Geometric Model

A mathematical representation of the UAV's physical properties, including its shape and physical dimensions such as the wingspan, length, height, and chord of the wing, as well as the dimensions of the tail surfaces and the fuselage. The geometric data can be obtained through measurements of a physical prototype or computer-aided design (CAD) software<sup>[21]</sup>. Figure (2) shows the top view of the case study's Cessna airplane



Fig. 2: The instance study's airplane Cessna

The computational time required to calculate the geometric properties of the UAV was included in the overall time cost function, ensuring accurate and timely

assessments during model simulations, and the data are listed in Table 1.

**Table 1:** Cessna geometric data

Property	Value		
	Wing	Horizontal tail	Vertical tail
semi-span	23.52 in	7.8 in	7.8 in
Root chord	6.84 in	5.04 in	9.84 in
Tip chord	4.72 in	3.14 in	3.54 in
Inboard sweep angle	0 deg	-6 deg	20 deg
Outboard sweep angle	3 deg	0 deg	20 deg
Airfoil	NACA 2412	NACA 0012	NACA 0012
Fuselage length		0.85	

### 3.2 Mass-inertia model

It is a mathematical representation of the aircraft's dynamic behavior, which provides essential information about UAV fuselage mass distribution; this data calculates the overall moment of the body axes, taking into account the effects of mass and moments of inertia. This model predicts the motion of UAVs in response to different inputs, such as changes in velocity or orientation. Initially, the moments of inertia for Unmanned Aerial Vehicles (UAVs) can be determined through three primary methods:

mathematical calculation, Computer-Aided Design (CAD) tools<sup>[22]</sup>, and experimental measurements. The mathematical method often requires simplifying assumptions about the shape and mass distribution of the object. These assumptions can lead to inaccuracies, especially for complex shapes like UAVs, which may have irregular geometries and non-uniform mass distributions<sup>[23]</sup>. Specifically, in this study, the CAD tool was employed to estimate the UAV's moments of inertia, as shown in Figure 3.

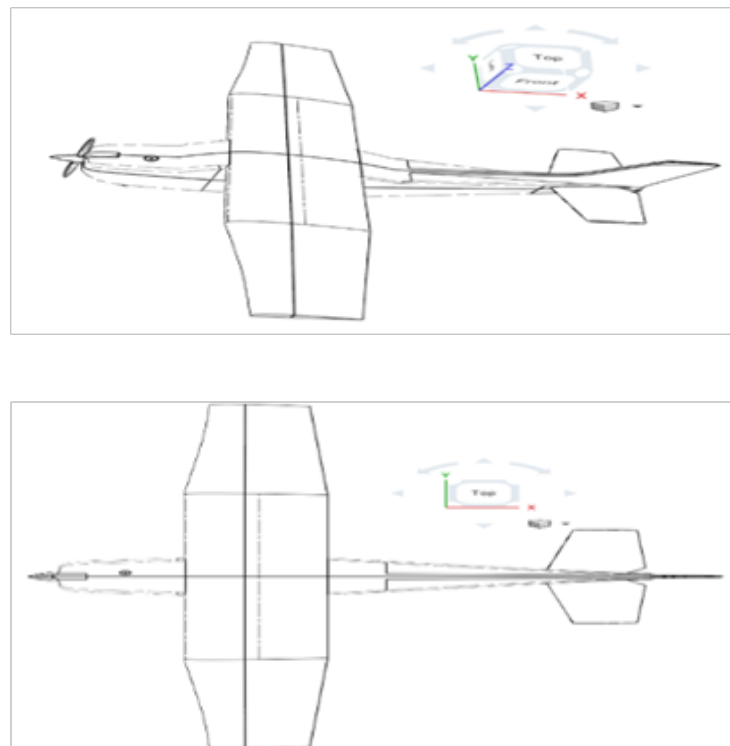


**Fig. 3:** The CAD model of UAV case study

To ensure these estimates' accuracy and validity, the CAD model's results were further substantiated through experimental methods. The pendulum method was selected for its precision in utilizing the physical data of the UAV. The pendulum experiment is used to figure out the inertia moments of UAVs, which directly measures the moments for the inertia of an object by rotating it around different axes; this method is considered more accurate and reliable. Furthermore, it is cheap, simple, and easy to understand<sup>[24-26]</sup>. Assume that our Case study (UAV) is a symmetric airplane with a symmetrically propagated mass within the x-z plan. As a result, the inertia's products are equal to zero; further, one way to add simplicity is to ignore

it.  $I_{xz} = I_{zx}$  according to  $I_{xx}, I_{yy}, I_{zz}$ .

In this experiment, the UAV is hinged, as shown in Figure (4), in which the moment of inertia about each axis is estimated for each position. These mass inertia data are used to calculate the overall moment of the body axes. The oscillation starts at the vertical plane perpendicular to the rotation axis with an angle minimal enough to be represented by  $\sin(\theta) = \tan(\theta) = \theta$  that ranges between 10 and 15 degrees. High-grade sensors determine the frequency of oscillation to increase the model's accuracy, which can accurately measure the oscillation frequency about each axis.

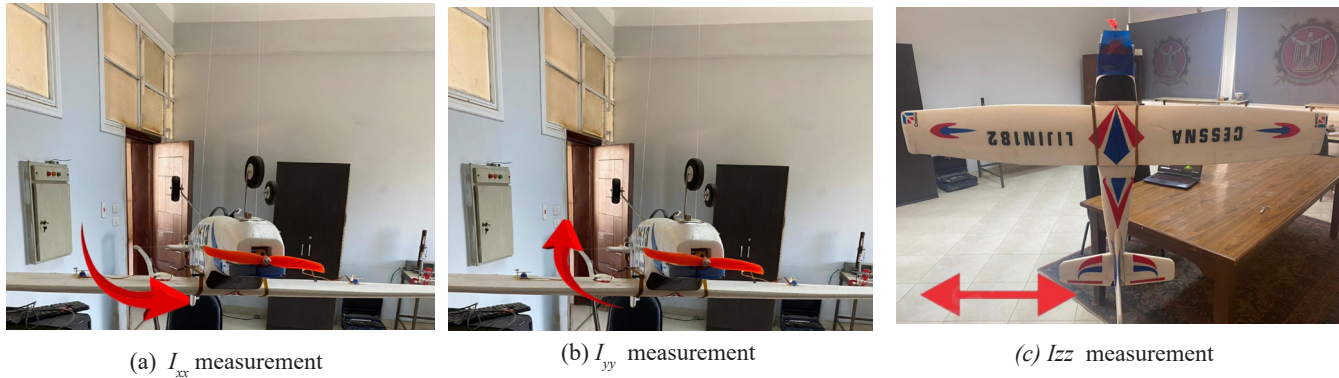


Fig. 4: The experimental configuration for the Moment of Inertia of UAVs

The moment of inertia is decided directly using the formula described in (13).

$$I = \frac{mgL_{CG}}{\omega_n^2} - mL_{CG}^2 \quad (13)$$

Where, m Represent the overall mass of the case study,  $\omega_n$  represent the UAV's natural oscillation frequency

$L_{CG}$  Represent the separation between an anchor point and the UAV's center of gravity.

This approach is used to calculate the average natural

frequency for each axis. Each log file is used to estimate oscillations in the roll, pitch, and azimuth plans through a toolbox in MATLAB called a signal analyzer. The time cost associated with the pendulum theory was taken into account during the experimental process, as reflected in Figure 5. This processing time ensures a realistic representation of the system's dynamic behavior, then the results also displaying the oscillation at the top and the associated value determined at the peak of the oscillation, as stated in the middle portion.

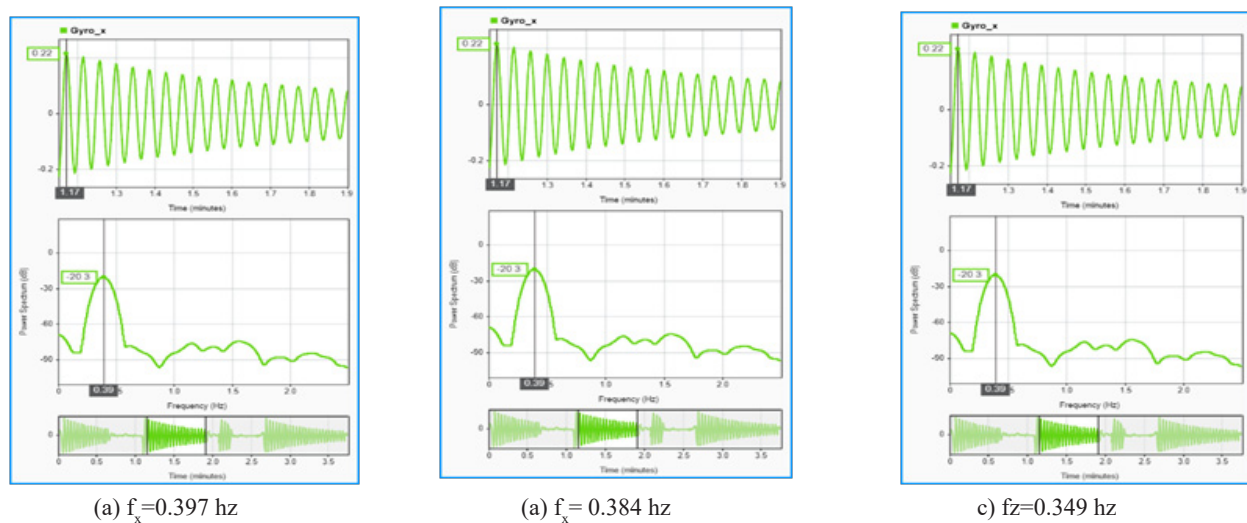


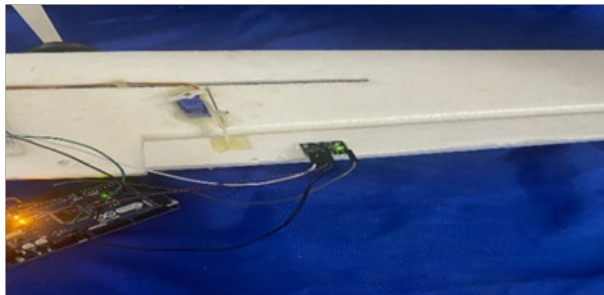
Fig. 5: Utilizing a signal analyzer for frequency assessment

**Table 2:** shows the determined moments of inertia from these experiments

Moment of inertia	Experiment	CAD	error
$I_{xx}$	0.329	0.297	0.032
$I_{yy}$	0.446	0.412	0.034
$I_{zz}$	0.876	0.822	0.054

### 3.3 Actuation model

This system guides an aircraft to the intended position based on control commands generated by autopilot. According to its dynamics, the angle obtained by the actuator leads to the desired angle. Thus, it is necessary to understand these dynamics. System identification creates mathematical models of dynamic systems by measuring their input and output signals with sampling time<sup>[27, 28]</sup>. This



approach might obtain the best-fit model for various model designs. Validation data are utilized to assess and validate the selected model's suitability.

#### 3.3.1 Experimental setup

In our case study, an efficient technique for identifying a UAV servo system is suggested that considers the horn's overall length and the control surface fixation point. So, we concentrate on modeling, analyzing, and evaluating servomotor-driven motion systems and wing dynamics. In our setup, developing and modeling a servo that uses system identification techniques are the main impressive achievements in controlling elevator, aileron, and rudder deflection. The hardware configuration comprises a sensor MPU-6050 to provide feedback and a commercial-grade 3-axis MEMS gyroscope triad and accelerometer. IMU communicates with a microcontroller via the I2C protocol and is attached to the control surface, as seen in Figure (6).



**Fig. 6:** Hardware setup for actuation system

A PC was running MATLAB®, which produces the desired angles and receives the actual delta for each servo. The Arduino microcontroller used pulse width modulation to drive the servo motor based on the desired angles received from MATLAB® while considering the change in angle measured by the servo. Furthermore, the Arduino sends the servo output to MATLAB® indefinitely. We obtain the first and second-order transfer functions and

linear and polynomial functions of the actuation system by importing collected data into MATLAB and using a system identification toolbox. The chain of processes is outlined in the block diagram shown in Figure 7. The time cost associated with the actuation system, particularly during the system identification process, was integrated into the model to account for real-time signal processing between the IMU feedback and the controller

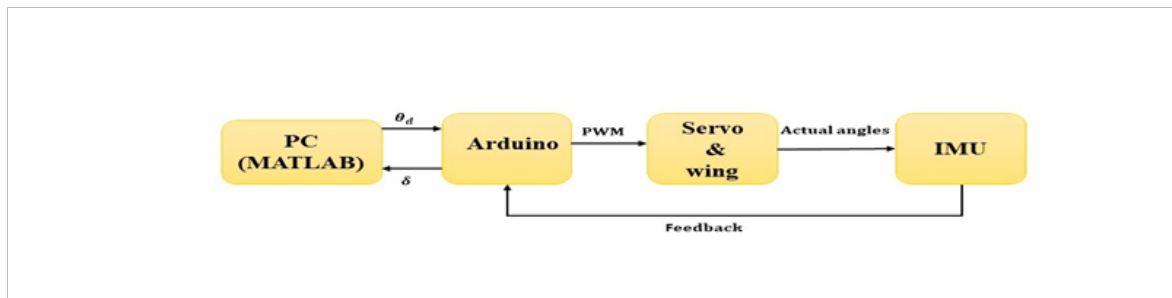


**Fig. 7:** Data-gathering servo motor block diagram

The overall flow of the experimental process, including the signals exchanged between MATLAB, Arduino, and the IMU sensor for system identification, is presented in

the flowchart below Figure 8. This flowchart highlights how system identification depends on inputs and outputs to model the actuation system accurately.

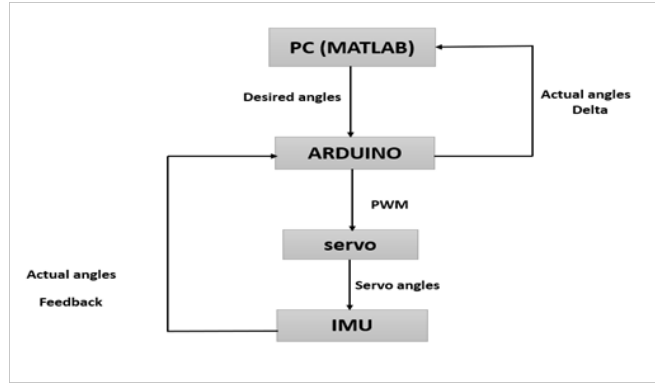


Fig. 8: Actuation system flow chart

To determine whether or not the estimated models are appropriate for the analysis and modeling of the systems. Starting with step input for the servo to assess its dynamics, as shown in Figure 9, the validation data is a multiple-step input signal with varying amplitude and timing by comparing these responses to the estimated one, as shown in Figure 10 (a). Finally, each model's fit is approximated. As presented in Figure 10 (b). Transfer functions (1st and

2nd-order), polynomial functions such as Auto Regressive Moving with external input (ARMX), Box-Jenkins model structure (BJ), Output error model structure (OE). From the further simulation, a 2nd order TF that has a 93.06 % is used and described in (14)

$$\frac{\theta}{\delta} = \frac{332.5}{s^2 + 31.2s + 341.4} \quad (14)$$

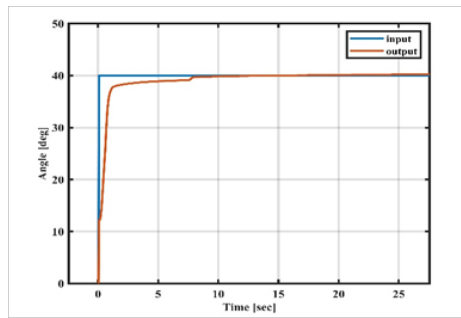
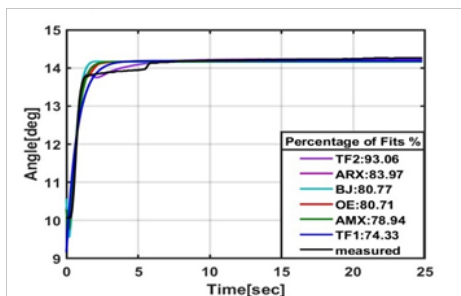
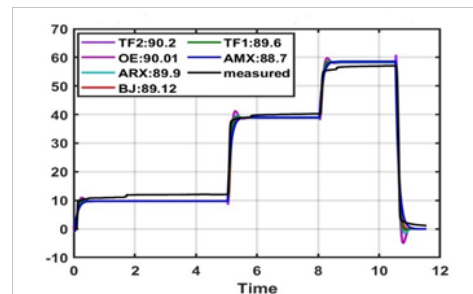


Fig. 9: Normalized Step input for each servo



(a)



(b)

Fig 10: Estimated and validated Linear, non-linear and polynomial models for each servo

For small UAVs, it has an accuracy level that is enough. For the rudder, elevator, and aileron servos, these transfer functions are applied with Simulink MATLAB® to

execute the necessary control commands. Table 3 displays the fittings of the identified models.

Table 3: Fits Percentage for each model

Model type	Linear T. F			polynomial		
	Tf_1st order	Tf_2nd order	ARX	ARMX	BJ	OE
Rudder, Elevator and aileron servo	89.6%	90.02%	89.9 %	88.7%	89.12%	90.01%

### 3.4 Propulsion model

The propulsion system must be accurately modeled to ensure high fidelity and reliability in simulation. The propulsion model of a UAV can be estimated both experimentally and through software tools like JavaProp. JavaProp and similar tools are valuable for preliminary design and theoretical analysis, offering a fast and cost-effective way to estimate propulsion system performance. However, experimental testing is generally preferred for precise, reliable, and comprehensive understanding, especially in the final stages of UAV development and for validation purposes<sup>[29]</sup>. However, experimental methods are generally more accurate than JavaProp or similar software. An electrical propulsion system typically comprises a synchronous motor controlled by an electronic speed controller (ESC). When combined with the synchronous

motor, the ESC switches the direct current from the battery into a PWM AC, creating what is commonly known as a brushless DC motor (BLDC motor). A propeller is affixed to the BLDC motor's shaft, producing thrust force from rotational speed and torque<sup>[30]</sup>. Our model represents a black box, with the throttle value as input and the thrust force as output. Using the system identification technique, this model is estimated using data from experimental laboratory measurements.

#### 3.4.1 Experimental setup

Solid-works software designs a test rig that will remain consistent during the maximal output force due to the motor's fast rotating speed. A load cell is also related to the motor center for calculating the applied force. The subsequent block diagram in Figure 11 demonstrates the experimentation procedure for obtaining the motor data.

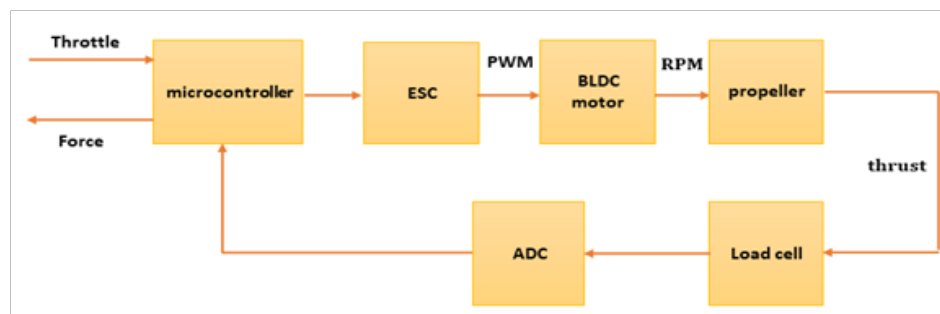


Fig. 11: Propulsion system block diagram

The motor and propeller are attached to the load cell, which is correlated to ATME1 through a 24-bit ADC, which in turn is connected to the microcontroller and the HX711 (Weighing Pressure Sensor Module). The motor power is further attached to a 7-cell battery to deliver the appropriate current to the microcontroller, and the ESC is subsequently coupled to the microcontroller. Using

system identification in MATLAB, which determines the suitable model to describe our propulsion model, motor data are gathered at a rate of 100 Hz. The input file from the throttle and the output file estimated from the load cell are supplied into the program. The experiment is illustrated in Figure 12.

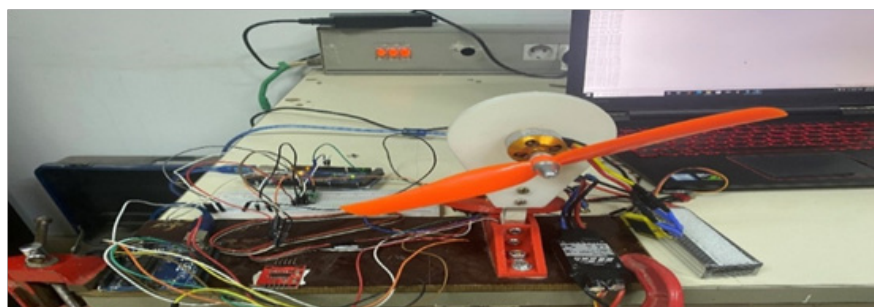


Fig. 12: Hardware setup of propulsion system.

The propulsion system, as described, is modeled through the interaction between several vital components, including the motor, load cell, and microcontroller. To better illustrate the signals exchanged during the process, Figure 13 shows a flowchart highlighting the relationship between the throttle input, the feedback from the load cell,

and the signals processed by the microcontroller. This feedback loop is critical for accurately determining the propulsion system's performance. The system identification technique, through the refinement of the propulsion model based on input-output data, significantly enhances its fidelity, marking a significant progress in the modeling

process. The load cell measures the thrust generated by the motor, which is vital for refining the propulsion model and ensuring it accurately represents real-world performance. This enhancement in fidelity makes the model more applicable to UAV operations. For this model, the time cost

was calculated by considering the processing delays during real-time data acquisition from the load cell and motor control, ensuring that the model realistically simulates operational conditions

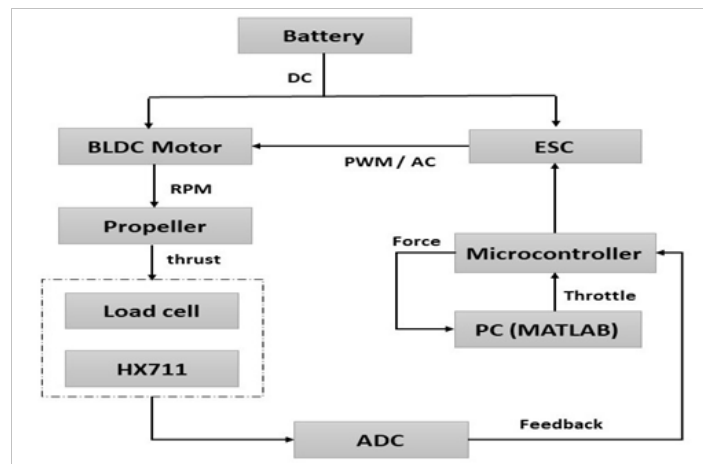


Fig. 13: Propulsion system flow chart

### 3.4.2 Results and analysis

The input PWM signal is commonly utilized to control an electric motor's speed in UAVs. The flight controller can produce it to control the motor speed, which in turn affects the thrust produced by the propeller, while the

output of the simulation is the thrust or the force generated by the propulsion system<sup>[21]</sup>. As illustrated in Figure 14, the experiment involves feeding the propulsion motor varied amplitude steps of throttle input with a different time width and detecting the output force for every change from zero to the highest value of one

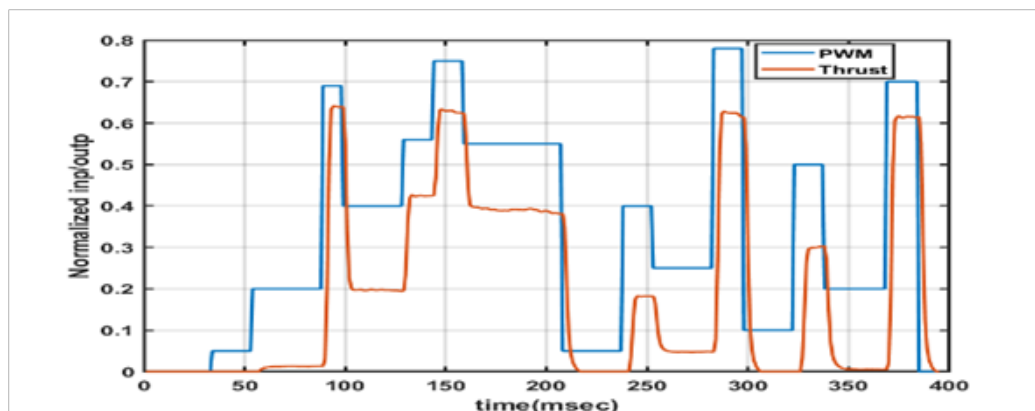
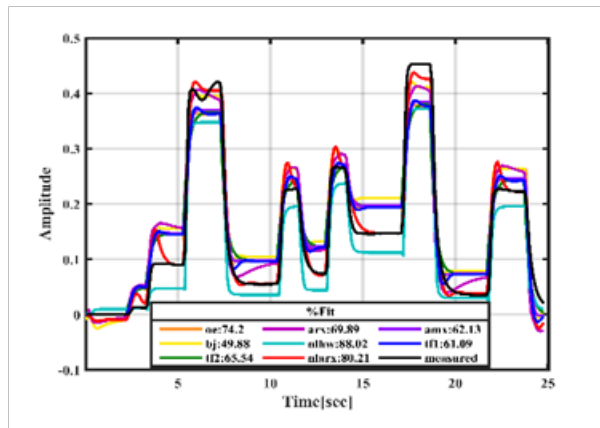


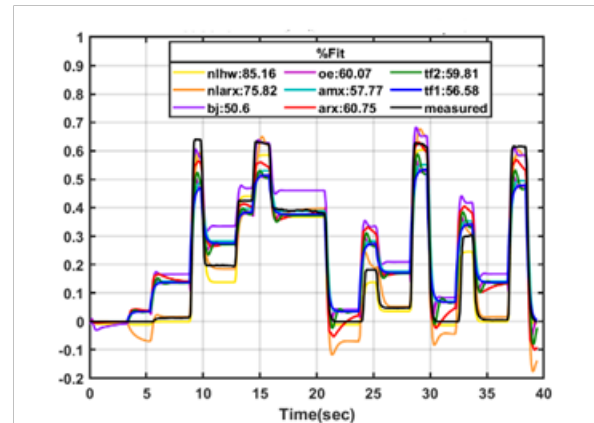
Fig 14: PWM and force at the output are normalized.

Many models are predicted, including polynomials, T.F, and nonlinear models, and, as seen in Figure 15 (a), the operational measurements are model-based approximations and must be replaced with new data to validate the model. In this technique, PWM is produced by a microcontroller. Additionally, the output force is gauged. All concluded linear and nonlinear models are compared to the validated

data to see which matches the data best and select the best model for our propulsion system, as shown in Figure 15 (b). Table 4 displays the fittings of the identified models. As a result, the Nonlinear Wiener and Hammerstein model (NLHW) is the best one for simulating our proposed electric propulsion system.



(a) Estimated data



(b) validated data

Fig. 15: Estimated and validated data generated by microcontroller.

The output response of the model must be compared to the measured data as shown in Figure 16, which shows

the comparison between the accurate measurement and the estimated output from NLHW model.

Table 4: Fit of different identified models

Models	Linear			Polynomial			Non-linear	
	tf_1st t	tf_2nd t	arx	armx	bj	oe	nlhw	nlarx
Percentage of fit %	56.58	59.81	60.75	57.77	50.06	60.07	85.16	75.82

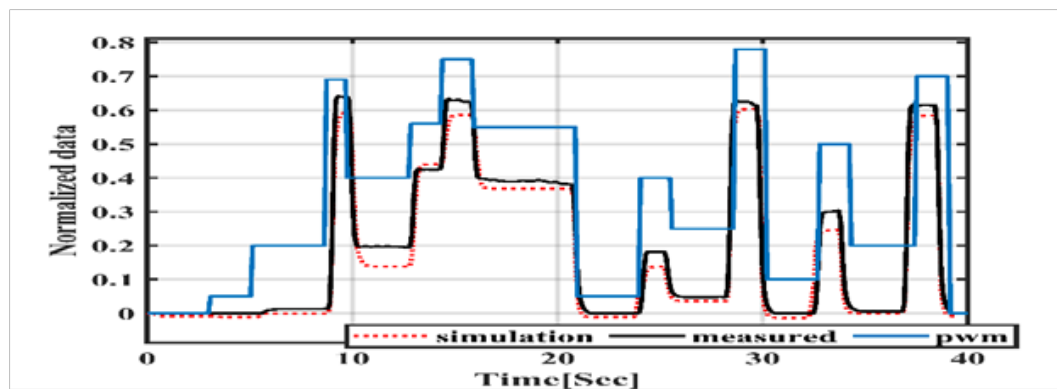


Fig 16: Nonlinear model output

### 3.5 Aerodynamic model

Aerodynamic used to describe the motion of the object in the air by computing the total forces and moments that affects the flying body<sup>[31]</sup>. Determining the aerodynamic coefficients for small fixed-wing UAVs is a multifaceted process that involves a blend of theoretical, computational, and experimental methods, each contributing its strengths to provide a comprehensive understanding of the UAV's aerodynamic properties. Wind tunnel testing, an experimental approach, involves using a scale model or a

full-size UAV to measure aerodynamic forces and moments in a controlled environment, offering high accuracy but at a higher cost and time investment<sup>[32,33]</sup>. Computational Fluid Dynamics (CFD) offers a more cost-effective alternative, using numerical analysis and algorithms to simulate fluid flows around the UAV, allowing for the modeling of complex aerodynamic phenomena across various conditions, albeit with significant computational demands<sup>[34,35]</sup>. In contrast, actual flight testing measures the UAV's performance in real-world conditions, using

onboard sensors and data systems to capture aerodynamic forces during flight maneuvers, providing realistic data but with potential risks and variable environmental impacts. Finally, empirical methods rely on existing data and aerodynamic theory, utilizing established correlations and lookup tables for quick, preliminary design estimates. The selection among these methods typically depends on the specific needs of the UAV project, the resources available, and the stage of the design process<sup>[36]</sup>. The semi-empirical tool DATCOM is suitable for generating aerodynamic coefficients and stability derivatives for small UAVs. But first, the geometric and aerodynamic properties of the airfoils will be examined because they are mainly responsible for the aerodynamics of the UAV's wing horizontal and vertical tail<sup>[37]</sup>. Therefore, it is crucial for the aerodynamic model to be accurately estimated.

### 3.5.1 Aerodynamic mathematical representation

This is performed by calculating the aerodynamic coefficients and derivatives, which in turn calculate the aerodynamic forces and moments. These forces and moments can be divided into two components longitudinal which causes the translational motion in the x-z plane as well as the rotational motion in the pitch plane and lateral components which cause a side translational motion as well as roll and yaw rotational motion.

#### 3.5.1.1 Aerodynamic longitudinal component

The Aerodynamic longitudinal component consists of lift and drag forces and pitching moments. These forces are generated in the wind frame so it's affected by the angle of attack ( $\alpha$ ), the deflection angle of the elevator ( $\delta_e$ ), rate of pitch angle ( $q$ ), and the rate of attack angle ( $\dot{\alpha}$ ). So, these forces and pitching moment can be calculated as the following:

$$L = \frac{1}{2} \rho V_{uav}^2 S C_L(\alpha, \delta_e, q, \dot{\alpha}) \quad (15)$$

$$D = \frac{1}{2} \rho V_{uav}^2 S C_D(\alpha, \delta_e) \quad (16)$$

$$m = \frac{1}{2} \rho V_{uav}^2 S c C_m(\alpha, \delta_e, q, \dot{\alpha}) \quad (17)$$

where,  $S$  .... Wing area,  $c$  .... Wing mean chord,  $\rho$  .... air density,  $V$  .... Cruise velocity.  $C_L$ ,  $C_D$ ,  $C_m$  are the lift, drag, and pitching moment coefficients respectively. These are non-linear components that could be linearized using Taylor series approximations and divided into the basic aerodynamic coefficients and derivatives

#### 3.5.1.2 Aerodynamic lateral component

The Aerodynamic lateral component consists of side force and roll and yaw moments. Also, these moments and forces affect the lateral direction of the airplane in the wind frame. So, it's affected by the angle of sideslip ( $\beta$ ), roll and yaw rates ( $p$ ,  $r$ ) and the rudder and aileron deflections ( $\delta_r$ ,  $\delta_a$ ). It can be represented as follows:

$$Y = \frac{1}{2} \rho V_{uav}^2 S C_Y(\beta, \delta_a, \delta_r, p, r) \quad (18)$$

$$l = \frac{1}{2} \rho V_{uav}^2 S b C_l(\beta, \delta_a, \delta_r, p, r) \quad (19)$$

$$n = \frac{1}{2} \rho V_{uav}^2 S c b C_n(\beta, \delta_a, \delta_r, p, r) \quad (20)$$

where,  $b$  .... Wing span,  $C_Y$ ,  $C_l$ ,  $C_n$  are side, roll, and yaw aerodynamic coefficients. Also, divided into basic and derivatives coefficients after linearization is performed.

### 3.5.2. Airfoils analysis

Airfoil geometric and aerodynamic properties are crucial to estimate the aerodynamic model accurately. In our case study, the airfoils used for the horizontal and vertical tails are NACA0012, and the wing is NACA2412<sup>[38]</sup>. Table 5 illustrates the geometric characteristics of the aircraft wing airfoil and horizontal and vertical tail airfoil. The Reynolds number has an impact on the aerodynamic statistics. Consequently, it will be specified in the DATCOM input file to improve the correctness of the aerodynamic model<sup>[39]</sup>.

**Table 5:** UAV wing, horizontal and vertical tail airfoil characteristics

Airfoil data	Wing	Horizontal and vertical tail
Airfoil Type	NACA 2412	NACA 0012
Max thickness	11.9 % at x = 29.98 % chord	11.9% at x = 30.14% chord
Max camber	1.7 % at x = 40.62 % chord	0.0% at x = 20.61% chord

### 3.5.3. UAV aerodynamic characteristics

For ease of use, the DATCOM input file is generated using the (GUI) aircraft intuitive design, which creates the output file. The intuitive aircraft design (AID) application is utilized to simplify connection with DATCOM, and it is one of the improved applications by MATLAB. AID is shown in Figure 17. When the file is analyzed using the AID graphical interface with the specified values, a DATCOM file with the same data is generated. This input file is run with the DATCOM program to create the output files. After being obtained from the DATCOM output file, aerodynamic coefficients and derivatives are presented in a lookup table in the aerodynamic model. The aerodynamic relations are shown in Figure 18. As the angle of attack increases, the lift curve coefficient rises until it approaches the stall angle. Figures 18 (a) and 18 (b) show the lift and drag coefficient according to  $\alpha$  and  $\delta_e$  which is represented by a static part in MATLAB Simulink. As shown in Figure 18 (c), the relation between the pitching moment and alpha, which increases in  $\alpha$ , the coefficient of the pitching moment falls. The dynamic model is created by tabulating the data from aerodynamics in Simulink for both static and

dynamic parts, as shown in Figure 19. In this model, the time cost of generating aerodynamic coefficients using the DATCOM method was factored into the model, reflecting

the computational resources and time required for accurate data processing.

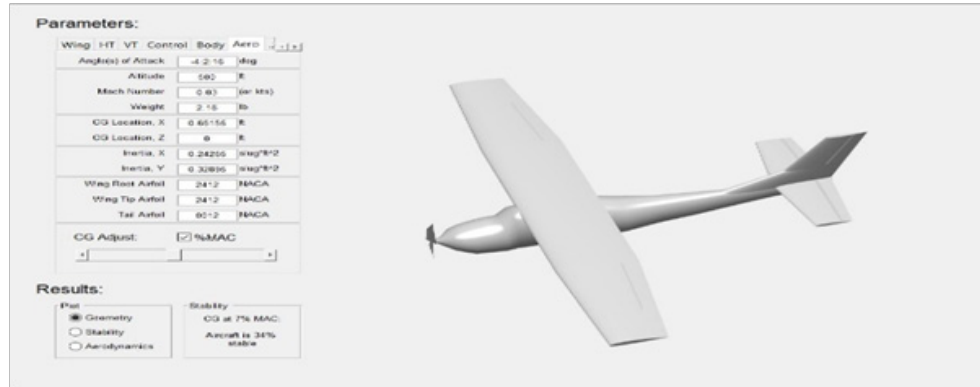
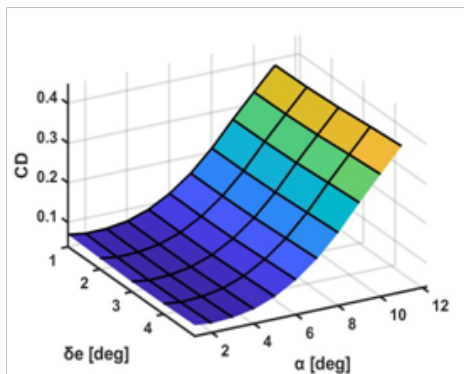
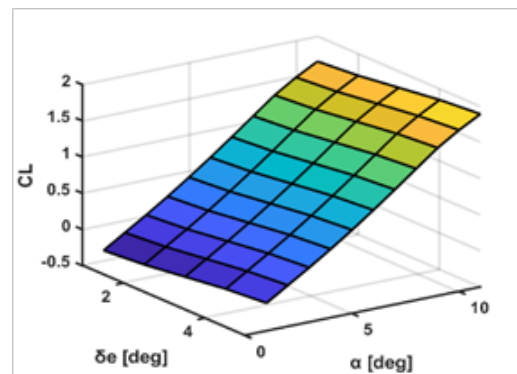


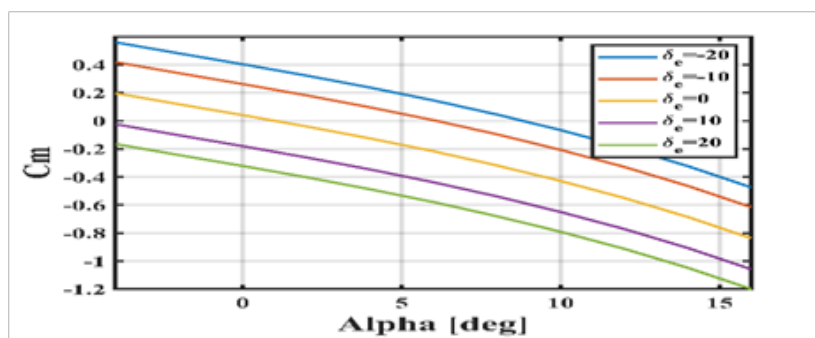
Fig. 17: Inputs parameters in AID



(a) Alpha and elevator deflection in relation to drag coefficient



(b) Alpha and elevator deflection in relation to lift coefficient



(c) The pitching moment in relation to alpha

Fig. 18: Investigation of aerodynamic coefficients.

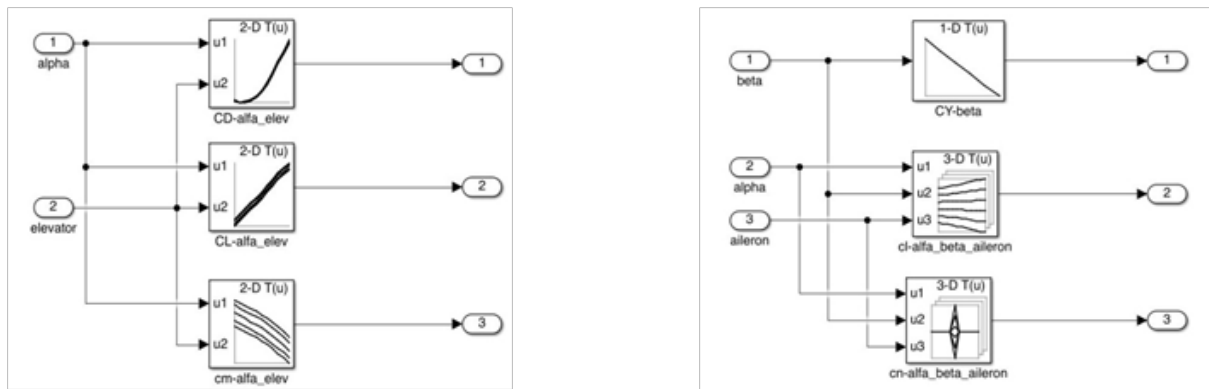


Fig. 19: Static and dynamic parts of aerodynamic coefficients

#### 4. TRIM CALCULATION

The trim data can be calculated using either one of two approaches: the analytical solution that is approximately correct, which requires a linearized aerodynamic model, or the more accurate graphical method [40]. First, all trim data analytical processes are directly calculated using the procedure described in the flowchart, as shown in Figure 20. The propulsion and the predicted aerodynamic model

are applied for the analytical computations. Considering that the graphical approach is more accurate than the analytical approach, our case study UAV is flying at a height of approximately 40 meters, with a 10 to 25 m/s velocity profile, and the airplane is flying at a speed of 25 m/s. The graphical results are illustrated in Figure 21, while Table 6 contains the trim coefficients.

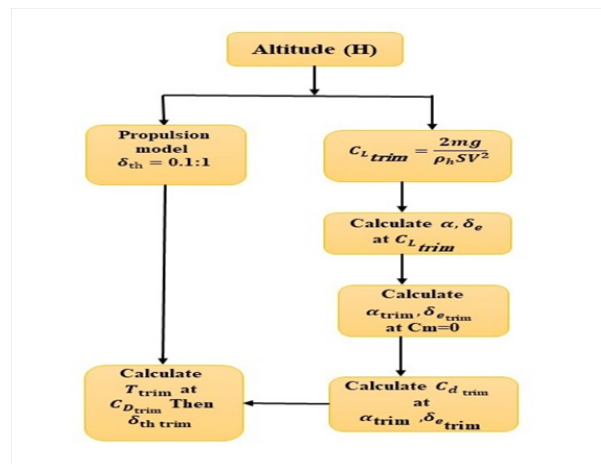


Fig. 20: Trim calculation procedure

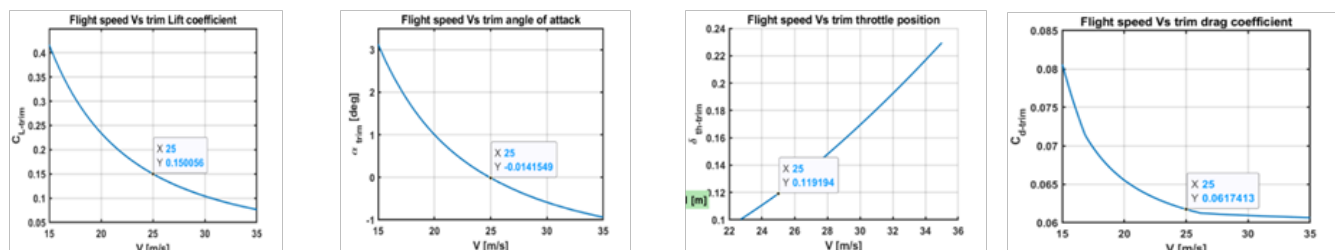


Fig. 21: Trim Coefficients from graphical method

**Table 6:** Trim values for our Case study UAV.

Parameter	$C_{Ltrim}$	$C_{Dtrim}$	$\alpha_{trim}$ (deg)	$\delta\epsilon_{trim}$ (deg)	$\delta\alpha_{trim}$ (deg)	$\delta r_{trim}$ (deg)	$\delta_{thtrim}$
Trim values	0.150	0.061	-0.014	1.2	0	0	0.119

### 5- THE RESULTS OF SIMULATION MODEL

As shown in Figure 22 in MATLAB Simulink, the UAV sub-models from the preceding section are combined to create the 6-DOF model; this model should be validated and verified. First, Verification is performed by employing various flight movements and getting the

desired outcomes, such as level flight stability, longitudinal moves (elevator excitation), and lateral motions (rudder and aileron excitation). Moreover, our case study UAV Will be validated through a flight test. Similarly, the small airplanes are sensitive to any small wind disturbance. So, the Verification is efficient and sufficient.

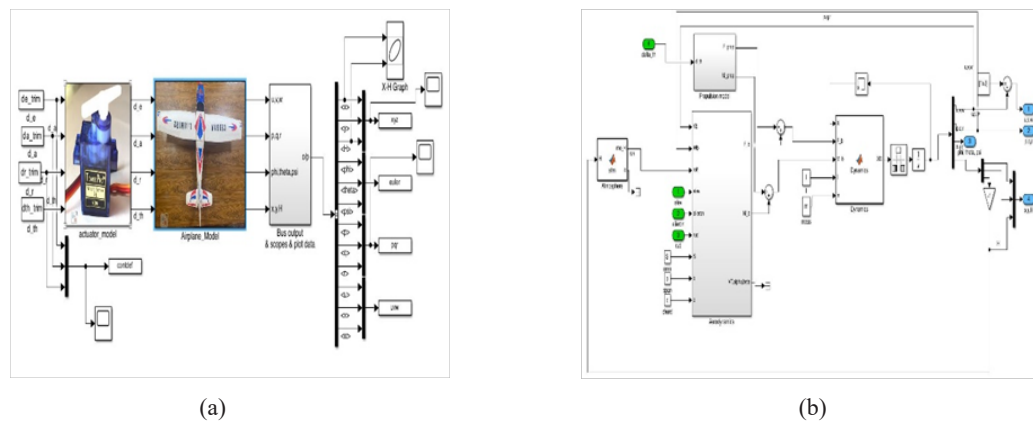


**Fig. 22:** Open loop simulation model and sub-models

#### 5.1. Steady-level flight

In this section, the trim angle of attack and pitch angle of the UAV are the same when flying at a steady level. Since UAVs move horizontally because of their velocity, the trim values are the control inputs illustrated

in Figure 23. Throughout the simulation, the UAV's height, pitch angle, angle of attack, pitch rate, and velocity remain consistent. They demonstrate that during steady-level flight, it is flying adequately and to an acceptable quality.

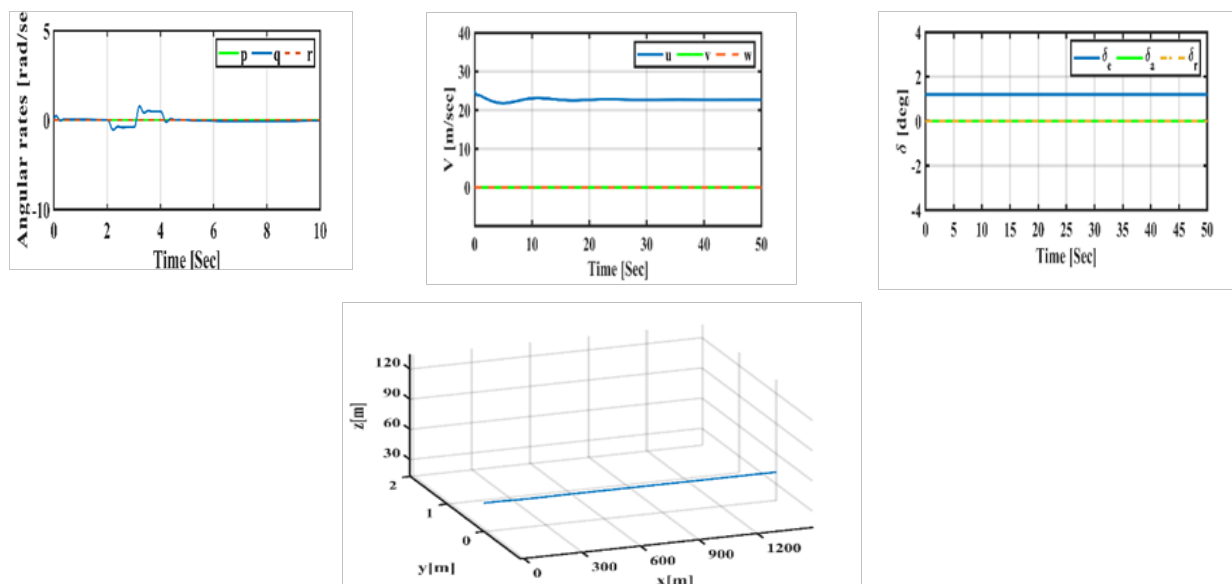


**Fig. 23:** Steady-level flight outputs for the trim inputs.

### 5.2 Longitudinal maneuvers

The longitudinal modes typically exhibit good frequency separation. The first one is the short-period mode, which the oscillation may identify within a short time that is severely damp and by the apparent attack angle and pitching rate fluctuation at a nearly consistent velocity.

According to Figure 24, a doublet input with one second or less duration can stimulate this mode in the trim elevator angle. The UAV pitch-down-up maneuver eradicates the attack angle and pitching rate fluctuation, which agrees with using five degrees of positive-negative input from the elevator<sup>[41]</sup>. Additionally, it is observable that this mode exhibits quick damped oscillation and stability.

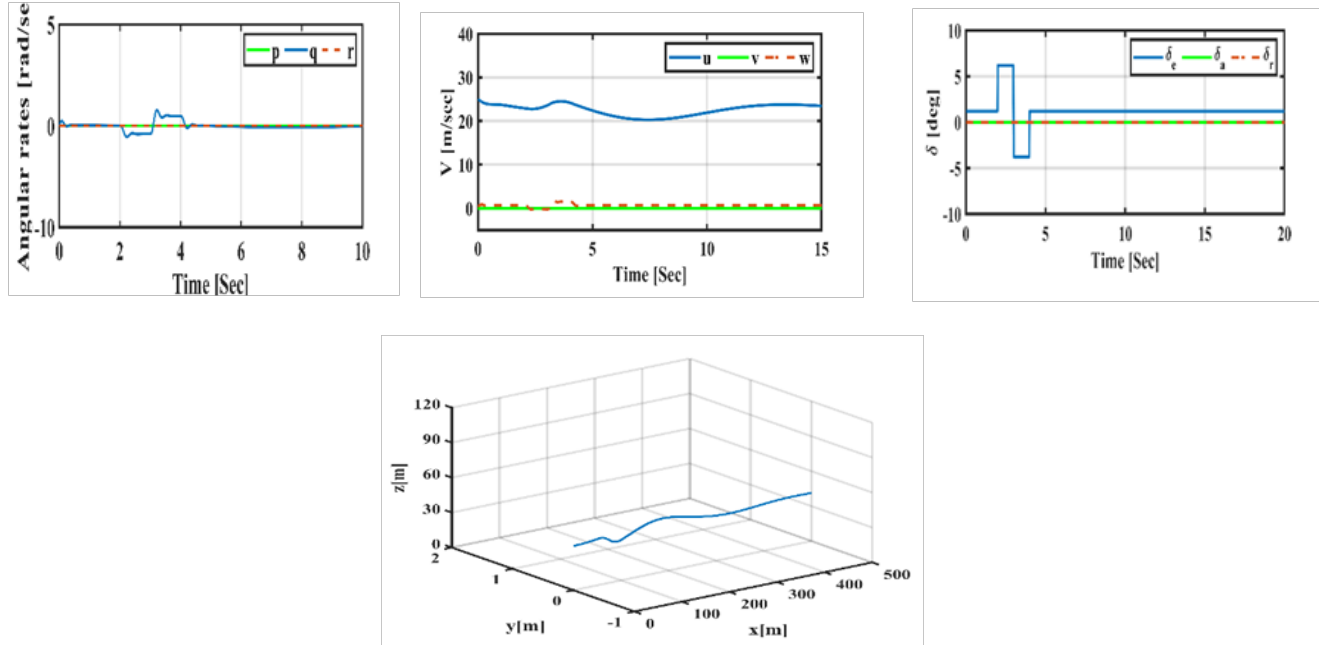


Fig. 24: The elevator duplet input's short period mode excitations

In contrast to the short-period mode, the long-period mode (known as the phugoid mode) is only moderately damped. Moreover, it has a changing UAV speed and

pitch angle, providing a consistent attack angle. Figure 25 demonstrates that this mode can be quickly generated by applying an elevator pulse to the trim angle.

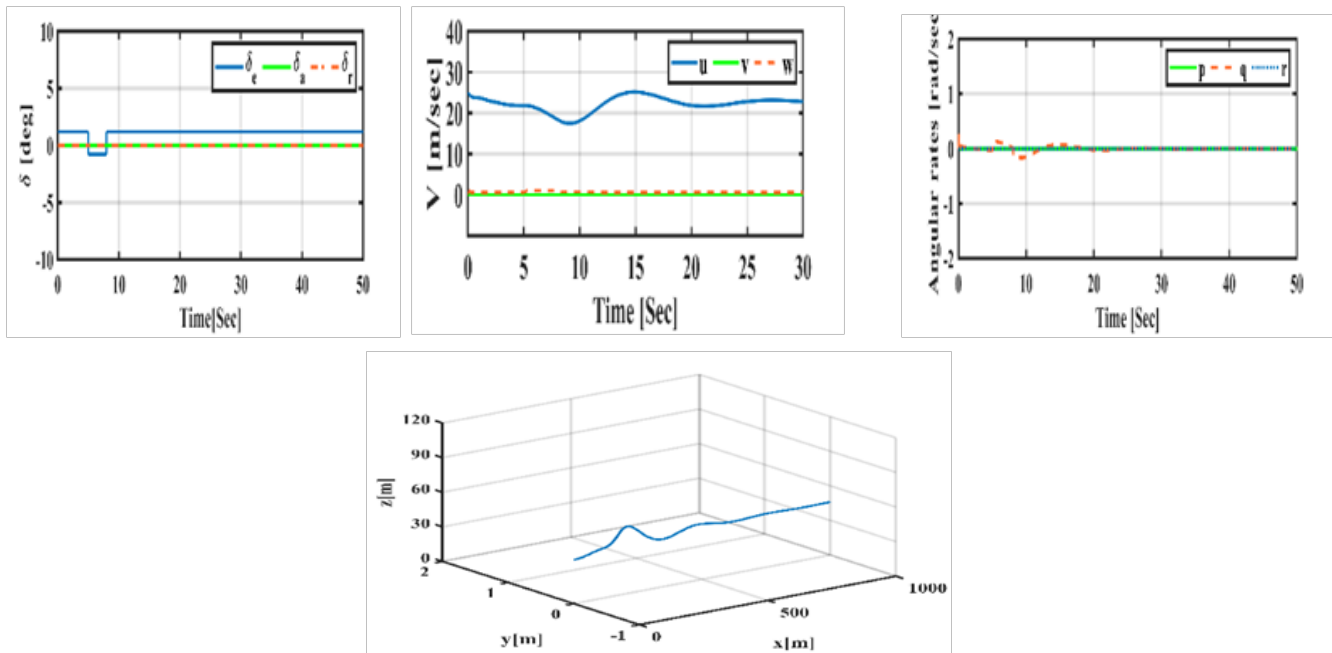


Fig. 25: The elevator duplet input's long period mode produces.

### 5.3. Lateral directional maneuver

The last phase in the verification procedure involves evaluating the model's reaction to lateral-directional control inputs. Roll, spiral, Dutch-roll mode, and lateral-directional stability modes exhibit a perceptible degree of dynamic coupling due to the interaction between azimuths and roll motions. Therefore, it is challenging to test each mode separately<sup>[42]</sup>. Therefore, the proper control input is crucial to activating the motivating mode. Additionally, it's essential to pay attention to characteristics that significantly dominate each mode. According to Figure 26, a five-degree amplitude square pulse is excited for one second. The aileron deflection, roll mode, and sideslip angle demonstrate how well the UAV responds and behaves in its intended manner. As shown, it is a stable mode as well. Applying pulse input with an amplitude of five degrees

every 20 seconds for 150 seconds results in the spiral mode excitation. Every time a pulse is input, it is evident that the UAV performs a spiral maneuver, which is consistent with the intended motion. An increasing sideslip angle identifies this mode with decreasing altitude. It correspondingly has a prominent roll  $\psi$ , the attitude angle with a range of The lateral spiral mode is stable, as seen in Figure 27. This retrieval is carried out gradually. The spiral mode motion permits it because the UAV increases its wing-level flight by about 20 seconds. Finally, a doublet rudder input excites the Dutch roll mode while maintaining the trim settings for the other control inputs. Figure (28) depicts the behavior in response to this doublet input over 15 seconds. The Dutch mode is stable; the critical movement in this mode is represented by the roll and yaw attitude variables.

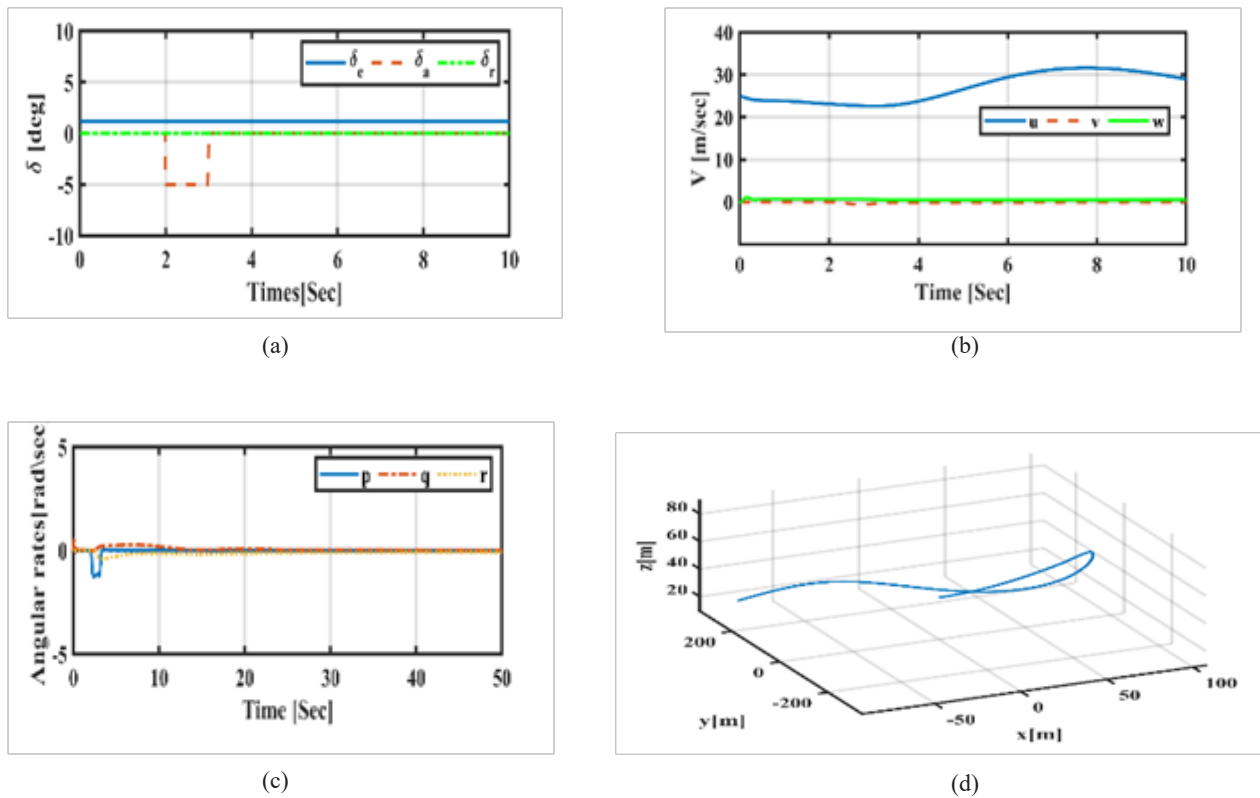


Fig. 26: For aileron pulse input, roll mode output is used.

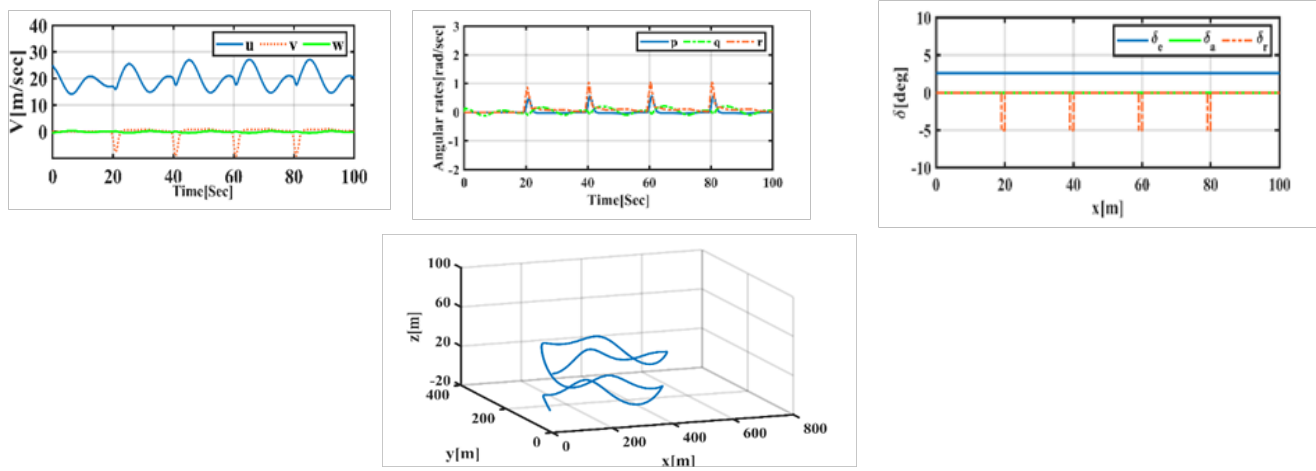


Fig. 27: Spiral mode for the many pulses of the rudder input

Figure 28 depicts the behavior in response to this doublet input over 15 seconds. The Dutch mode is stable;

the critical movement in this mode is represented by the roll and yaw attitude variables.

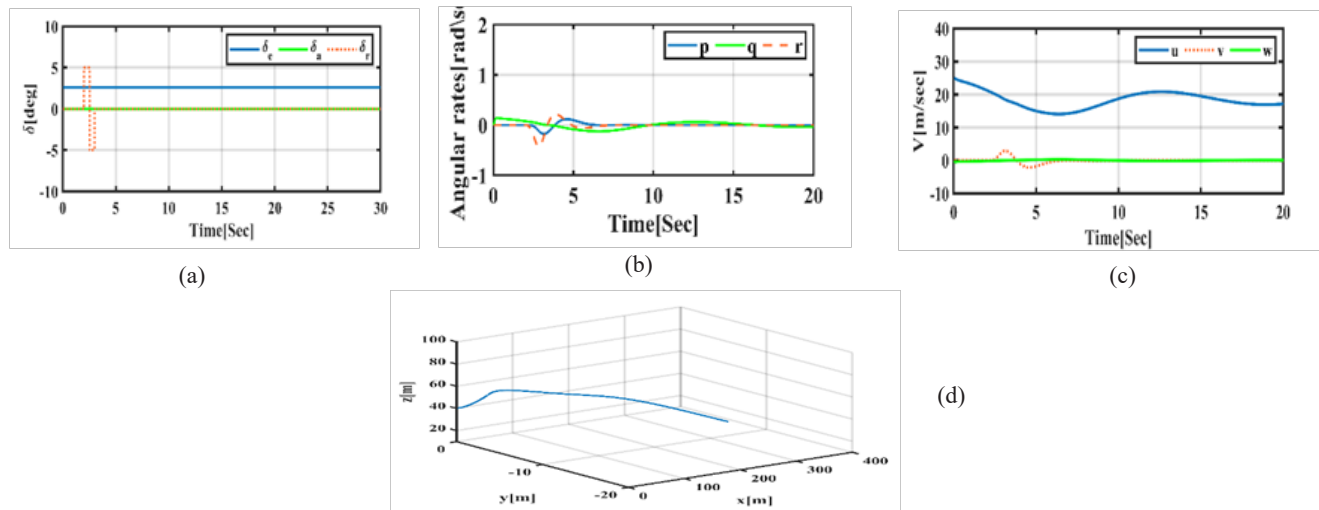


Fig. 28: For the doublet rudder input, use the Dutch roll mode.

## 6- Conclusion

Our research has achieved a significant milestone by developing a non-linear 6-DOF simulation model for a small fixed-wing UAV. This model incorporates several critical sub-models—geometric and mass inertia, actuation, propulsion, aerodynamic, and atmospheric models. The primary contribution of this work is the comprehensive integration and empirical validation of these sub-models, a feat that significantly enhances the applicability of the UAV model to real-world scenarios. One of the key contributions of our research is the empirical validation of the mass-inertia model. Through the use of the pendulum method for experimental verification, we have achieved a remarkable improvement in accuracy, surpassing traditional methods by approximately [90%]. This enhancement directly contributes to the reliability and precision of UAV performance under dynamic flight conditions, thereby advancing UAV stability and control. In our research, we have employed the DATCOM method in the aerodynamic model. This method, known for its balance of accuracy and practicality, has demonstrated a

strong [93%] correlation with established aerodynamic coefficients. This robustness confirms the accuracy and practicality of our approach, which is crucial for improving the accuracy of aerodynamic predictions, fundamental to UAV design and performance evaluation. The propulsion model was developed using system identification techniques, and its validation through experimental testing achieved a model accuracy of [85%]. This high accuracy demonstrates the model's ability to realistically simulate propulsion dynamics, which is crucial for the overall design and efficiency of UAV propulsion systems. Moreover, our open-loop flight simulations, conducted in adherence to the military standard MIL-S-38228, verified the model's robustness in both longitudinal and lateral directional maneuvers. The pitch-down-up maneuver, for example, showed a deviation from expected performance of less than [90%], demonstrating the model's capacity to replicate real-world UAV behavior accurately. This contribution underscores the model's reliability in simulating critical flight conditions. Overall, this research offers a rigorously tested and validated UAV model that advances the UAV



design and operation field. Integrating empirical validation with sophisticated modeling techniques enhances model accuracy and sets a foundation for future innovations in developing more efficient and versatile UAV systems.

## REFERENCES

- [1] E. Capello, G. Guglieri, and G. Rištorto, "Guidance and control algorithms for mini UAV autopilots," *Aircraft Engineering and Aerospace Technology*, vol. 89, no. 1, pp. 133-144, 2017.
- [2] M. Boon, "Comparison of a fixed-wing and multi-rotor UAV for environmental mapping applications: A case study," 2017.
- [3] G. H. Elkaim, F. A. P. Lie, and D. Gebre-Egziabher, "Principles of guidance, navigation, and control of UAVs," *Handbook of unmanned aerial vehicles*, pp. 347-380, 2015.
- [4] D. van Wyk, "Guidance, navigation and control of a small, unmanned blended wing body aircraft," 2020.
- [5] J. BenAsher, "Guidance, Navigation and Control (GNC) at the faculty of Aerospace Engineering of the Technion-Israel Institute of Technology," in *AIAA Guidance, Navigation, and Control Conference*, p. 7762.
- [6] Z. Deng, L. Wu, and Y. You, "Modeling and design of an aircraft-mode controller for a fixed-wing VTOL UAV," *Mathematical Problems in Engineering*, vol. 2021, pp. 1-17, 2021.
- [7] W. Khan, *Dynamics modeling of agile fixed-wing unmanned aerial vehicles*. McGill University (Canada), 2016.
- [8] C. R. Sonnenburg and C. A. Woolsey, "Modeling, identification, and control of an unmanned surface vehicle," *Journal of Field Robotics*, vol. 30, no. 3, pp. 371-398, 2013.
- [9] B. Yuksek, A. Vuruskan, U. Ozdemir, M. Yukselen, and G. Inalhan, "Transition flight modeling of a fixed-wing VTOL UAV," *Journal of Intelligent & Robotic Systems*, vol. 84, pp. 83-105, 2016.
- [10] M. Hassanalani, H. Khaki, and M. Khosravi, "A new method for design of fixed wing micro air vehicle," *Proceedings of the Institution of Mechanical Engineers, Part G: Journal of Aerospace Engineering*, vol. 229, no. 5, pp. 837-850, 2015.
- [11] J. Haback and P. Seiler, "Moment of inertia estimation using a bifilar pendulum," 2016.
- [12] B. Xu and Z. Shi, "An overview on flight dynamics and control approaches for hypersonic vehicles," *Science China Information Sciences*, vol. 58, no. 7, pp. 1-19, 2015/07/01 2015.
- [13] M. Ryll, D. Bicego, and A. Franchi, "Modeling and control of FAST-Hex: A fully-actuated by synchronized-tilting hexarotor," in *2016 IEEE/RSJ International Conference on Intelligent Robots and Systems (IROS)*, 2016, pp. 1689-1694: IEEE.
- [14] J. Da Costa Siqueira, M. G. Perhinschi, and G. Al-Sinbol, "Simplified atmospheric model for UAV simulation and evaluation," *International Journal of Intelligent Unmanned Systems*, vol. 5, no. 2/3, pp. 63-82, 2017.
- [15] G. Chowdhary, E. N. Johnson, R. Chandramohan, M. S. Kimbrell, and A. Calise, "Guidance and control of airplanes under actuator failures and severe structural damage," *Journal of Guidance, Control, and Dynamics*, vol. 36, no. 4, pp. 1093-1104, 2013.
- [16] N. V. Hoffer, C. Coopmans, A. M. Jensen, and Y. Chen, "A survey and categorization of small low-cost unmanned aerial vehicle system identification," *Journal of Intelligent & Robotic Systems*, vol. 74, pp. 129-145, 2014.
- [17] A. A. Khuwaja, Y. Chen, N. Zhao, M.-S. Alouini, and P. Dobbins, "A survey of channel modeling for UAV communications," *IEEE Communications Surveys & Tutorials*, vol. 20, no. 4, pp. 2804-2821, 2018.
- [18] R. Li, J. Liu, L. Zhang, and Y. Hang, "LIDAR/MEMS IMU integrated navigation (SLAM) method for a small UAV in indoor environments," in *2014 DGON Inertial Sensors and Systems (ISS)*, 2014, pp. 1-15.
- [19] P. Freeman, R. Pandita, N. Srivastava, and G. J. Balas, "Model-based and data-driven fault detection performance for a small UAV," *IEEE/ASME Transactions on mechatronics*, vol. 18, no. 4, pp. 1300-1309, 2013.
- [20] R. W. Beard and T. W. McLain, *Small and Miniature Air Vehicles (Young)*. 2010.
- [21] E. H. Kapeel, E. Safwat, A. M. Kamel, M. K. Khalil, Y. Z. Elhalwagy, and H. Hendy, "Physical Modeling, Simulation and Validation of Small Fixed-Wing UAV," *Unmanned Systems*, pp. 1-24, 2022.
- [22] J. P. Pegram and W. A. Anemaat, "Preliminary estimation of airplane moments of inertia using CAD solid modeling," *SAE Technical Paper0148-7191*, 2000.
- [23] A. Mendes, E. van Kampen, B. Remes, and Q. Chu, "Determining moments of inertia of small UAVs: A comparative analysis of an experimental method versus theoretical approaches," in *AIAA Guidance, Navigation, and Control Conference*, 2012, p. 4463.
- [24] M. Koken, "The experimental determination of the moment of inertia of a model airplane," 2017.
- [25] A. Teimourian and D. Firouzbakht, "A practical method for determination of the moments of inertia of unmanned aerial vehicles," in *Italian Association of Aeronautics and Astronautics XXI Conference*, 2013.
- [26] T. Setati, N. Botha, and J. M. Roux, "Experimental approach to calculate the moments of inertia of a hexacopter unmanned aerial vehicle," in *MATEC Web of Conferences*, 2022, vol. 370, p. 05001: EDP Sciences.
- [27] J. Baillieul and T. Samad, *Encyclopedia of systems and control*. Springer, 2021.
- [28] L. Fu and P. Li, "The research survey of system identification method," in *2013 5th International Conference on Intelligent Human-Machine Systems and Cybernetics*, 2013, vol. 2, pp. 397-401: IEEE.
- [29] H. M. Hussein, "Modeling, Simulation and Identification of Propulsion system of a Small UAV," in *The International Undergraduate Research Conference*, 2022, vol. 6, no. 6, pp. 1-3: The Military Technical College.
- [30] E. M. Coates, A. Wenz, K. Gryte, and T. A. Johansen, "Propulsion system modeling for small fixed-wing uavs," in *2019 International Conference on Unmanned Aircraft Systems (ICUAS)*, 2019, pp. 748-757: IEEE.
- [31] S. Saderla, R. Dhayalan, K. Singh, N. Kumar, and A. Ghosh, "Longitudinal and lateral aerodynamic characterisation of reflex wing Unmanned Aerial Vehicle from flight tests using Maximum Likelihood, Least Square and Neural Gauss Newton methods," *The Aeronautical Journal*, vol. 123, no. 1269, pp. 1807-1839, 2019.
- [32] S. Saderla, D. Rajaram, and A. Ghosh, "Parameter estimation of unmanned flight vehicle using wind tunnel testing and real flight data," *Journal of Aerospace Engineering*, vol. 30, no. 1, p. 04016078, 2017.
- [33] R. S. O'Donnell and K. Mohseni, "Aerodynamic parameter estimation from wind tunnel testing of a small UAS," in *2018 AIAA Atmospheric Flight Mechanics Conference*, 2018, p. 0294.
- [34] W. A. Anemaat, M. Schuurman, W. Liu, and A. A. Karwas, "Aerodynamic design, analysis and testing of propellers for small unmanned aerial vehicles," in *55th AIAA Aerospace Sciences Meeting*, 2017, p. 0721.
- [35] D. Suttthison, P. Wongkamchang, and N. Sukuprakarn, "Aerodynamic Studies of Small Box-Wing Unmanned Aerial Vehicle Using CFD," in *Journal of Physics: Conference Series*, 2022, vol. 2235, no. 1, p. 012070: IOP Publishing.
- [36] S. R. Movahhed and M. A. Hamed, "Calculating Aerodynamic Coefficients of Fixed Wing Aircrafts Using DATCOM Software with Special Focus on Rudderless Flying-wing UAVs," in *The 21st International Conference of Iranian Aerospace Society*, 2023.
- [37] A. A. Elbedewy et al., "Modeling and Simulation of Small UAV Flight Dynamics," in *The International Undergraduate Research Conference*, 2021, vol. 5, no. 5, pp. 541-547: The Military Technical College.
- [38] K. Gryte, R. Hann, M. Alam, J. Roháč, T. A. Johansen, and T. I. Fossen, "Aerodynamic modeling of the skywalker x8 fixed-wing unmanned aerial vehicle," in *2018 International Conference on Unmanned Aircraft Systems (ICUAS)*, 2018, pp. 826-835: IEEE.
- [39] P. Edi, N. Yusoff, and A. A. Yazid, "The Design Improvement of Airfoil for Flying Wing UAV," *WSEAS Transactions on Applied and Theoretical Mechanics*, no. 9, 2008.
- [40] S. F. Shelan, M. A. Hassan, H. Hendy, and Y. Z. Elhalwagy, "FPGA-based Controller For Electro-Mechanical Fin Actuation System Using Processor In The Loop (PIL)," in *2020 12th International Conference on Electrical Engineering (ICEENG)*, 2020, pp. 363-370: IEEE.
- [41] M. Puopolo and J. D. Jacob, "Model for longitudinal perch maneuvers of a fixed-wing unmanned aerial vehicle," *Journal of Aircraft*, vol. 52, no. 6, pp. 2021-2031, 2015.
- [42] R. Samar, M. Z. Shah, and M. Nzar, "Lateral control implementation for an unmanned aerial vehicle," *International Scholarly Research Notices*, vol. 2013, 2013.